Appl. Phys. B 55, 109–116 (1992)

Applied Physics B Photophysics and Laser Chemistry

Computational Chaos in Nonlinear Optics

M. Belić[1], Z. Ljuboje[1,*], M. Sauer[2], and F. Kaiser[2]

[1] Institute of Physics, P.O. Box 57, 11001 Belgrade, Yugoslavia, Fax: +11-108-198
[2] Institut für Angewandte Physik, Technische Hochschule Darmstadt, W-6100 Darmstadt, Fed. Rep. Germany, Fax: +6151-163279

Received 31 January 1992/Accepted 12 March 1992

Abstract. A few models of nonlinear optical systems, known experimentally to possess both stable and unstable dynamical modes, are approximated by different dynamical models and integrated by different numerical methods. It is shown that the onset of instabilities and chaotic behavior in the same physical system may be dependent on the model used and on the numerical method applied. Finite order difference schemes should be applied with caution to infinite dimensional dynamical systems displaying irregular behavior.

PACS: 42.50.Lc, 42.65.Hw

Great influence of computers on the development of deterministic chaos [1] is self-evident. The advent of the former triggered an explosion of interest in the latter. The past few decades exhibited an enormous increase in the number of publications dealing with chaos and in the number of people entering the research of chaotic phenomena. There are very few fields of human scientific endeavour not affected by deterministic chaos, that is, by the methods of nonlinear (NL) dynamics, and by computers.

This is especially befitting NL optics, which even boasts an adjective "nonlinear" in its name. Some of the most beautiful examples of chaotic motion came from NL optics. Almost all new ideas in the theory of chaos, from the early ones (such as period doubling in iterative maps) to the more recent ones (such as defect mediated turbulence) were speedily observed in NL optical systems. This very Special Issue testifies the strength and the breath of research into chaotic phenomena in optical systems.

However, when one relies on computer simulations, it happens that instead of observing chaos in a physical system, one observes chaos in the dynamical model used to describe the system or in the numerical method used to treat the model [2]. This may sound obvious to a NL dynamicist, but precisely because of enormous proliferation of chaotic research, we think that another reminder will not be out of order. Thus, we explore here the problems that may occur when one, without due caution, attempts to deal with NL optical systems using simplified models and methods.

The existence of such problems is known for long time. The original Lorenz model is known to be an incomplete approximation to the corresponding Navier-Stokes equations. The higher order models (the *5 component* or the *7 component*) offer different dynamical behavior in most cases. Consequently, our setting will be more restrictive. We will show that the same physical system, described by one and the same continuous dynamical model, but treated by different numerical schemes, may lead to different long-time behavior. Even though different numerical schemes can be understood as different discrete dynamical models, we prefer to refer to this as the computational chaos.

Different things might go wrong when one deals with the chaos on computers. First, and most benign, are the problems with the computers themselves. They possess finite machine (roundoff) error, finite memory, and operate on a finite range of rationals. Owing to the finite error and the finite observation time, there is no way to distinguish a very long periodic orbit from a quasiperiodic or a chaotic trajectory. However, usually something else goes wrong before one is confronted with the problems with computers. Nonetheless, it is very disturbing when the same algorithm executed on two different computers produces different results [3].

Second, and more often, there are the problems with numerics. Most come from inadequate discretisation of continuous temporal models. As a rule, iterative maps are poor approximations to real physical systems. Discretisation changes fundamentally the nature of a continuous dynamical model. There should be no problem as long as the limit $h \to 0$, where h is the integration step, recovers the continuous behavior. Unfortunately, such a limit may not be attain-

* Permanent address: "Zrak" Company, 71000 Sarajevo, Yugoslavia

able in a chaotic system. Chaotic behavior implies $t \to \infty$, and this cannot be reached when h is getting smaller.

The next set of problems is concerned with the overall numerical procedures by which chaos is obtained. Hereto belong steady-state analyses which yield multistability or chaos, or the fitting procedures in boundary value problems leading to chaos. To these also belong complicated discretisation procedures applied to partial differential equations or other infinitely dimensional dynamical systems. The examples presented in this paper are from this class of problems. We present three examples of spurious chaotic or multistable (periodic) responses of NL optical models. We stress the fact that the underlying physical systems are all displaying real, experimentally observed chaos in some regions of their parameter space.

The first two examples come from the field of optical phase conjugation (OPC) in photorefractive (PR) media [4]. During an OPC process a piece of PR crystal is illuminated by three laser beams: two counterpropagating pumps A_1 and A_2, and a signal A_4. Due to interaction of these fields, a fourth wave A_3 is generated in the crystal, counterpropagating to the probe A_4 and being its PC replica. The process is described by a set of four slowly-varying envelope wave equations, augmented by two-point boundary conditions. One of the examples displays the emergence (or suppression) of chaos through a process of ever more accurate solution procedure for the wave equations. The other displays the appearence of multistabilities and chaos during the process of fitting boundary conditions.

The third example comes from the field of optical bistability (OB) in NL optical ring resonators. A transverse extension of the Ikeda model [5] is treated by two different numerical algorithms: an FFT-based beam propagation method [6] and a Crank-Nicholson (CN) procedure. While the differences could be surmised to exist all the way to the chaotic region, we depict only the differences in P4 (period-4) solutions, which qualitatively look very similar, but belong to conceptually very different classes of solutions. A similar type of argument ("qualitatively similar, but in detail wrong") could be applied to all examples presented.

The paper is divided into five sections. Sections 1 and 2 contain presentations of the OPC examples, Sect. 3 contains a presentation of the OB example, and Sect. 4 offers some conclusions.

1 Computational Chaos in Optical Phase Conjugation

OPC in PR media is described by the following set of wave equations in the plane wave and one grating limit [7]:

$$\partial_z A_1 = Q A_4\,, \qquad \partial_z A_4^* = -Q A_1^*\,, \tag{1a}$$

$$\partial_z A_2^* = -Q A_3^*\,, \qquad \partial_z A_3 = Q A_2\,, \tag{1b}$$

where the derivative is in the propagation direction and Q is the amplitude of the (transmission) grating which has developed in the crystal. The amplitude of the grating satisfies a dynamical equation of its own:

$$\tau \partial_t Q + \varepsilon Q = \frac{g}{I}(A_1 A_4^* + A_2^* A_3)\,, \tag{2}$$

where τ is the relaxation time, ε is a parameter dependent on various internal electric fields (describing photorefractive crystals according to the theory of Kukhtarev et al. [8]), g is the wave-coupling parameter, and $I = \Sigma |A_i|^2$ is the total intensity. The detailed dependence of these parameters on electric fields is of no interest here. It suffices to say that when there is an external field applied to the crystal, parameters ε and g are complex numbers, otherwise they are real. It is known [7] that this system is apt to develop instabilities, and the extra phase shift introduced by the external electric field exerts a profound influence on the irregular behavior.

We treat (1) and (2) using increasingly more accurate numerical methods and monitor changes this procedure is causing in the behavior of the system. Temporal derivatives in (1) are neglected, due to slow response of the crystal, which is described by the relaxation-type equation (2). It can be assumed that the wave amplitudes are following adiabatically the formation of gratings. This separation of temporal and spatial derivatives allows a convenient integration procedure, in which time is divided into small intervals, and in each interval the process is considered as a diffraction of waves by the quasi stationary grating amplitude. Our interest is not focused on the detailed z-dependence of the fields, but on the dynamics of the OPC process.

The treatment of the dynamical equation (2) proceeds along the following lines. In the simplest approximation, an iterative map is constructed:

$$Q_{n+1} = \frac{g}{\varepsilon I}(A_1 A_4^* + A_2^* A_3)_n\,. \tag{3}$$

The procedure is to start the iterative loop with some arbitrary chosen value Q_0 and to iterate until a stable fixed point, or a periodic orbit, or a chaotic response is obtained. In between iterations, the fields are calculated by solving (1), either analytically (for g real), or by a fourth order Runge-Kutta (RK) algorithm, or by a shooting procedure. If there exists a fixed point of the map, then a unique solution is found; if there is a fixed point of the composed map (i.e., the map iterated a certain number of times), a periodic orbit is obtained. We point out that unique solutions are the same, regardless of the method by which they are obtained. The problems arise with instabilities.

In the next approximation, (2) is integrated formally as a first-order linear differential equation:

$$Q(t) = \exp\left(-\frac{\varepsilon}{\tau}t\right)\left[Q(0) + \int_0^t \frac{q(t')}{\tau}\exp\left(\frac{\varepsilon}{\tau}t'\right)dt'\right], \tag{4}$$

where q is an abbreviation for $g(A_1 A_4^* + A_2^* A_3)/I$. Assuming that q is approximately constant across the (small) time interval, one obtains:

$$Q(t+\Delta t) = \frac{q(t)}{\varepsilon}\left[1 - \exp\left(-\frac{\varepsilon \Delta t}{\tau}\right)\right] + \exp\left(-\frac{\varepsilon \Delta t}{\tau}\right)Q(t)\,. \tag{5}$$

A convenient feature of this formula is its natural dependence on the discretisation parameter $\Delta t/\tau = h$. Presumably, the most accurate results are obtained when $h \to 0$. The worst case is when $h \to \infty$, and this corresponds to

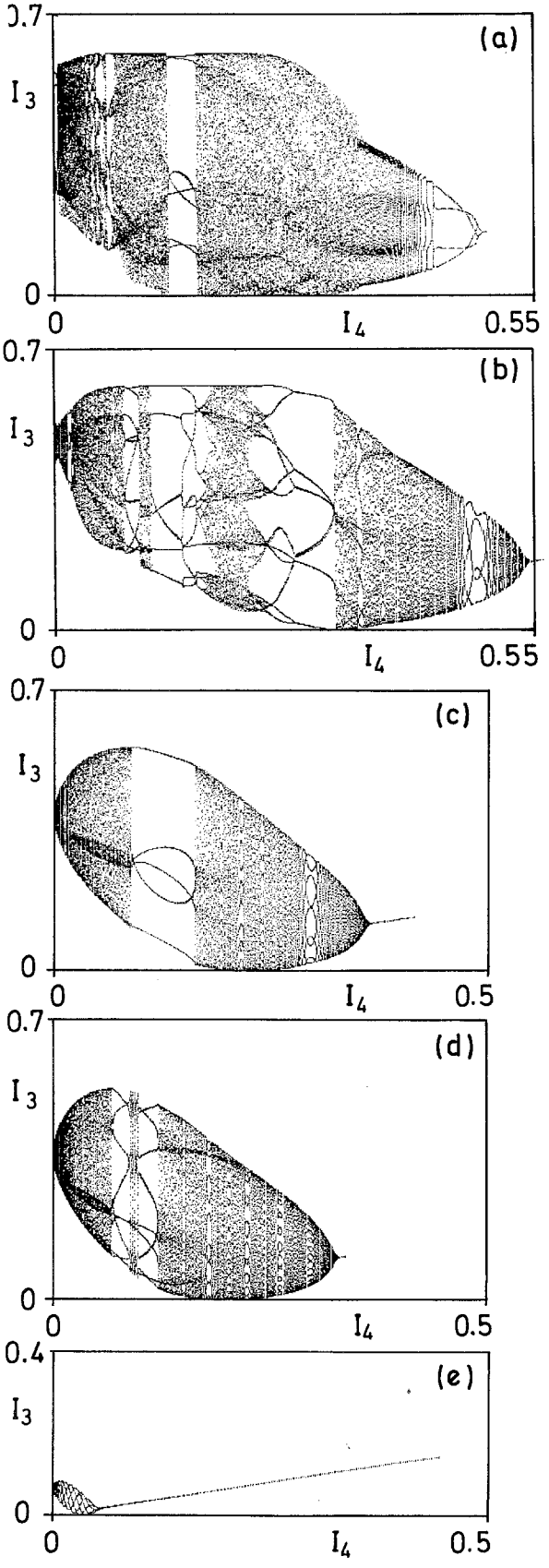

Fig. 1a–e. Bifurcation diagrams of the PC wave intensity I_3 as a function of the input signal intensity I_4 for different values of the discretisation parameter h. **a** $h = \infty$, the map (3); **b** $h = 33$, RK method; **c** $h = 25$, the same method; **d** $h = 25$, the map (6); **e** $h = 1$, RK. The other parameters are: $\varepsilon = (0.0598, 0.0186)$, $g = (0.0654, -0.2068)$ (complex numbers), $C_1 = 0.25$, $C_2 = 0.64$

steady-state, i.e., to the map from (3). In this manner a generalized map in the complex plane is formed:

$$Q_{n+1} = \frac{q_n}{\varepsilon}\left[1 + \exp(-\varepsilon h)\right] + \exp(-\varepsilon h)\, Q_n\,, \tag{6}$$

with h being the principal control parameter. Below we depict how different choices of h affect the behavior of the PC wave.

As a next refinement, a RK algorithm is applied to (2). Qualitatively, similar behavior is observed. In the end, a fairly complicated code is applied to the full system of equations (1) and (2), in which the spatial part is treated by a two-point shooting procedure, and the dynamical part is followed by an RK algorithm. Many of the instabilities observed by simpler models are suppressed, but, as reported [7], chaos can still be found for some values of parameters. These instabilities, however, are not more realistic than the ones seen in simpler models.

Figure 1 presents bifurcation diagrams which depict the PC intensity I_3 as a function of the signal intensity I_4. The series of figures displays suppression of instabilities as the accuracy parameter h and the methods are varying. For the chosen set of parameters there is no chaos in the original model. The most varied behavior is visible in Fig. 1. Going to the left from unique solutions (limit cycles), the first instability noted in all cases is quasiperiodic motion on a torus. This motion is interrupted by a number of periodic windows. Some windows open through frequency locking, some open through inverse intermittency. Ones that open through intermittency, close by executing period doubling to chaos. Thus, the whole wealth of chaotic phenomena can

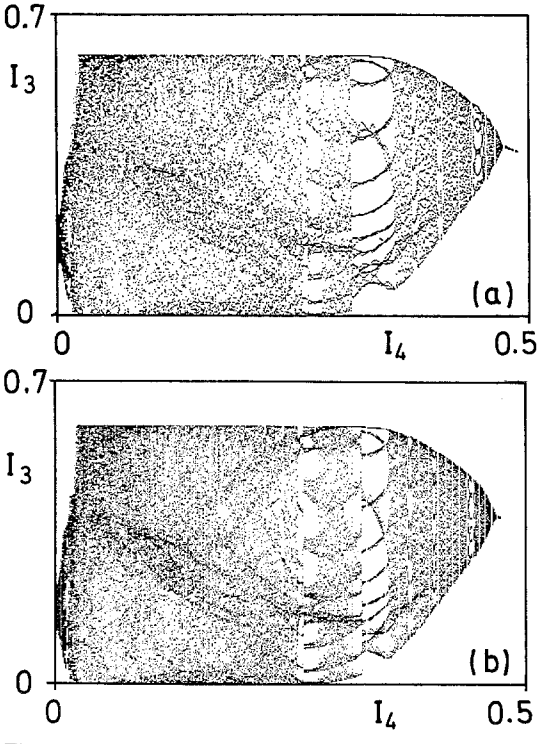

Fig. 2a, b. Bifurcation diagram for **a** the map, and **b** RK method, when g is large. As compared with Fig. 1, the diagram has become more chaotic as g increased. Here $\varepsilon = (0.6636, 0.0737)$, $g = (2.993, -6.6173)$, and $h = 1$

be observed in the case of computational chaos. Numerical instabilities follow the same routes to chaos as do the real physical systems.

Figure 2 shows an example of chaos in the underlying dynamical model. It is obtained by increasing the wave coupling parameter g, and displayed by using two different numerical procedures: RK and (5). Qualitatively, and even in the detail, the diagrams are very similar. There is less order for large g, which corresponds to high dimensional chaos. We defer discussion until Sect. 4.

2 Chaos in a Boundary Value Problem

Our second example from OPC deals with multistability and chaos obtained through a fitting procedure for boundary-value problems. The system is similar to the one described by (1) and (2), except that the two-wave mixing of the pumps is added and both transmission and reflection types of gratings are assumed to be present. The corresponding equations are of the form:

$$I\partial_z A_1 = g(Q_T A_4 - Q_R A_3) - \gamma I_2 A_1\,, \tag{7a}$$

$$I\partial_z A_2^* = g(Q_T A_3^* - Q_R A_4^*) - \gamma I_1 A_2^*\,, \tag{7b}$$

$$I\partial_z A_3 = -g(Q_T A_2 + Q_R^* A_1)\,, \tag{7c}$$

$$I\partial_z A_4^* = -g(Q_T A_1^* + Q_R^* A_2^*)\,, \tag{7d}$$

where $Q_T = A_1 A_4^* + A_2^* A_3$ and $Q_R = A_1 A_3^* + A_2^* A_4$ are the steady-state grating amplitudes, and γ is the two-wave mixing parameter. Note that now steady-state equations are considered, and at least part of the problems with multistabilities stems from this fact. This system is described in more detail in [9].

The intensity part of the solution of (7) can be written in terms of two functions v and w:

$$I_1 = I_{4d}\frac{u(v) - (v+\delta)}{2}\,, \qquad I_2 = I_{4d}\frac{u(v) + (v+\delta)}{2}\,, \tag{8a}$$

$$I_3 = I_{4d}\frac{\cosh w(v) - 1}{2}\,, \qquad I_4 = I_{4d}\frac{\cosh w(v) + 1}{2}\,, \tag{8b}$$

which are given as quadratures:

$$w(v) = \int_1^v \frac{f(x)}{xu(x)}\,dx\,, \tag{9a}$$

$$\ln v(z) + \int_1^v \frac{\cosh w(x)}{u(x)}\,dx = 2g(z-d)\,, \tag{9b}$$

where $f(v) = av^{\gamma/2g}$, $u(v) = [(v+\delta)^2 + f^2]^{1/2}$, and $I_{4d} = I_4(z=d)$.

In this manner, the original two-point boundary value problem is transformed into an initial value problem. The values of both variables are known on the $z = d$ face of the crystal: $v_d = 1$, $w_d = 0$, however, the input parameters a and δ, which figure in (9) through f and u, depend on the missing boundary values, and so do the intensities as well. The evaluation of a and δ is provided by a self-consistent iterative map procedure. Sometimes during this procedure unstable situations arise, leading to chaotic output.

The values of a and δ could be given in terms of the missing values I_{1d} and I_{4d} on the $z = d$ face of the crystal:

$$a^2 = \frac{4C_2 I_{1d}}{I_{4d}^2}\,, \qquad \delta = \frac{C_2 - I_{1d}}{I_{4d}} - 1\,. \tag{10}$$

Likewise, they could be given in terms of I_{20} and I_{30} (or, equivalently, v_0 and w_0) missing on the $z = 0$ face:

$$a^2 = 4C_1 C_2 x\,\frac{x(C_1 + C_2) + v_0 - 1}{C_1 + C_2 v_0^b}\,,$$
$$\delta = \frac{x(C_2^2 v_0^b - C_1^2) - C_1 v_0 - C_2 v_0^b}{C_1 + C_2 v_0^b}\,, \tag{11}$$

where $x = v_0(\cosh w_0 + 1)/2C_4$ and $b = \gamma/g$. C_1, C_2, and C_4 denote the given boundary conditions for intensities. Note that $C_3 = I_3(z=d) = 0$. The problem of fitting boundary conditions is resolved as follows. One starts by choosing arbitrary initial values for a and δ; from these I_{1d} and I_{4d} are calculated using (10). I_{20} and I_{30} (i.e., v_0 and w_0) are found by evaluating the integrals in (9). This enables the calculation of the new values for a and δ by (11), and the procedure is repeated until convergence. In this manner, a map is defined in the parameter plane and the procedure corresponds to the evaluation of the fixed points of the map. An interesting question is what happens if the map becomes unstable.

The instabilities set in for $g > 2$ and are investigated by standard methods of nonlinear dynamics, i.e., by evaluating the fixed points of the map and of its arbitrary compositions. Such fixed points may reveal the nature of the transition to chaos, if there is one. However, seeing such instabilities in a map does not mean that they exist in a real crystal, nor that they exist in the continuous model. This is a familiar danger when instabilities follow from a steady-state analysis and not from a time-dependent (dynamical) treatment of the process. An illuminating discussion of this point can be found among von Neumann's collected works [10]. The existence of such instabilities should be verified experimentally.

A phase diagram for a set of parameters is shown in Fig. 3. A typical bifurcation diagram around the chaotic region is depicted in Fig. 4. Thus, stable and unstable solutions are found depending on the strength of couplings. Different types of unstable behavior are observed: quasiperiodic motion on a torus and period doubling to chaos. Chaotic behavior in this context means that the intensity reflectivity does not settle onto any particular value. Even though each of these values represents an allowed solution to the boundary value problem at hand, it is unlikely that all of them are dynamically accessible to the system.

The procedure presented here allows one to obtain multistable or chaotic solutions from a stead-state analysis. The situation is similar to computational fluid dynamics, where multiple solutions are found to the stationary potential flow equation with given boundary conditions. The spurious solutions could not be invalidated within the mathematical model or numerical procedure, but with the use of an external thermodynamical criterion – the entropy production principle. This is what von Neumann and von Karman had to say about the multiplicity problem in a discussion at a conference in 1949 [10]:

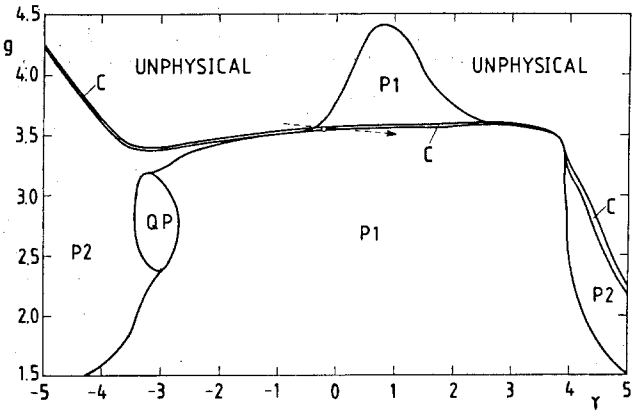

Fig. 3. Phase diagram in the $\gamma - g$ plane for $C_2 = 3$ and $C_4 = 0.6$. QP denotes the quasiperiodic region, and C denotes the chaotic band in which period doubling to chaos takes place. The region in which a^2 becomes negative is labeled UNPHYSICAL. In this region intensities become negative, and the model fails

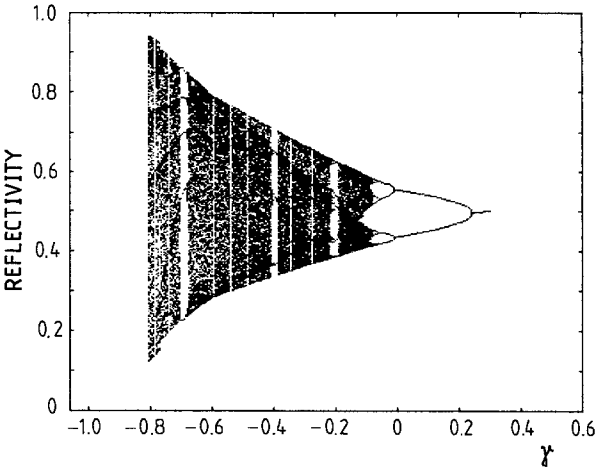

Fig. 4. A typical bifurcation diagram obtained by crossing the chaotic band from Fig. 3. This diagram corresponds to the horizontal dashed line in Fig. 3

Von Neumann: "The question as to whether a solution which one has found by mathematical reasoning really occurs in nature, and whether the existence of several solutions with certain good or bad features can be excluded beforehand, is a quite difficult and ambiguous one. One must be terribly careful in accepting such extra solutions."

Von Karman: "I would like to say something about this question of uniqueness of solutions. I don't think that there is any reason that if you put a problem in a form which has no physical meaning, there shall not be two solutions. And I think the case of stationary motion as such belongs to this category, because it can occur only as a limiting case."

Similar reasoning could be applied to our system. Instabilities found are obtained through a mathematical procedure. Steady-state situation has been assumed. There might exist physical criteria not contained in the model which could preclude the development of instabilities. Long time instabilities obtained in the systems in which temporal derivatives are neglected from the beginning, can lead to spurious solutions and chaotic scenarios that are not observed in real life. This question, in our opinion, is inadequately addressed in the literature.

3 Transverse Instabilities in Ring Resonators

The last example deals with a passive optical system consisting of a ring cavity and a homogeneously broadened 2-level medium. The model has been presented in detail elsewhere in this Special Issue [11]. It is concerned with the appearence of periodic spatial structures due to transverse mode instabilities. This phenomenon is known as the cooperative frequency locking [12]. A particular aspect of this phenomenon is considered, namely the symmetry breaking of the mode profile under the influence of spatial transverse modulation. This aspect is sensitive to numerical handling.

The model is a standard ring cavity of a length L containing a medium of thickness d [5]. The paraxial wave equation for a single transverse mode is given by

$$\left(\mathrm{i}\partial_z + \frac{1}{2k}\partial_x^2\right) E_n(x,z) = -\frac{\mathrm{i}\alpha(1+\mathrm{i}\Delta)}{2}\,\frac{1}{1+4I_n}\,E_n(x,z)\,, \tag{12}$$

where E_n is the electric field after n resonator passes, k is the wave number, α the absorption coefficient, and Δ the atomic detuning. The corresponding boundary conditions are given by

$$E_n(x,0) = T^{1/2}A(x) + R\exp(\mathrm{i}kL)E_{n-1}(x,d)\,, \tag{13}$$

where T is the transmittivity of the input mirror, R is the overall reflectivity of mirrors comprising the cavity, and $A(x)$ is the input beam profile. A Gaussian profile is chosen for A, with added harmonic modulation of the form:

$$A(x) = A_0[1 + A_m\cos(k_m x)]\exp(-x^2/\sigma^2)\,. \tag{14}$$

Thus, the model possesses inversion symmetry about the center of the beam. We are interested in the spontaneous breaking of this symmetry.

The model is treated numerically using two independent methods: a CN algorithm and a beam propagation method based on the fast Fourier transform (FFT). The general agreement between the two methods is very good, especially in the case of unique solutions and low periodic orbits. However, for higher orbits and higher Fresnel numbers of the cavity, considerable differences appear. While these differences should be expected in chaotic regions, where at most one can expect qualitative agreement, we present here a low periodic case, where numerical differences lead to qualitatively different solutions. This is the case for P4 solutions for $A_0 = 0.85$, $A_m = 0.15$, $k_m = 10$, and $\sigma = 0.06$. The other parameters are: $T = 0.1$, $R = 0.9$, $kL = 0.4$, $\alpha L = 0.01$, and $\alpha L\Delta = 10$.

It should be noted that the general behavior of the intracavity field on the lower OB branch and in the absense of modulation, changes from a fixed point to P2 and P4 orbits and then via a quasiperiodic region to chaos, as the amplitude A_0 of the input beam is increased. This behavior is the same for both numerical methods. As the modulation is turned on, however, a new qualitative moment appears:

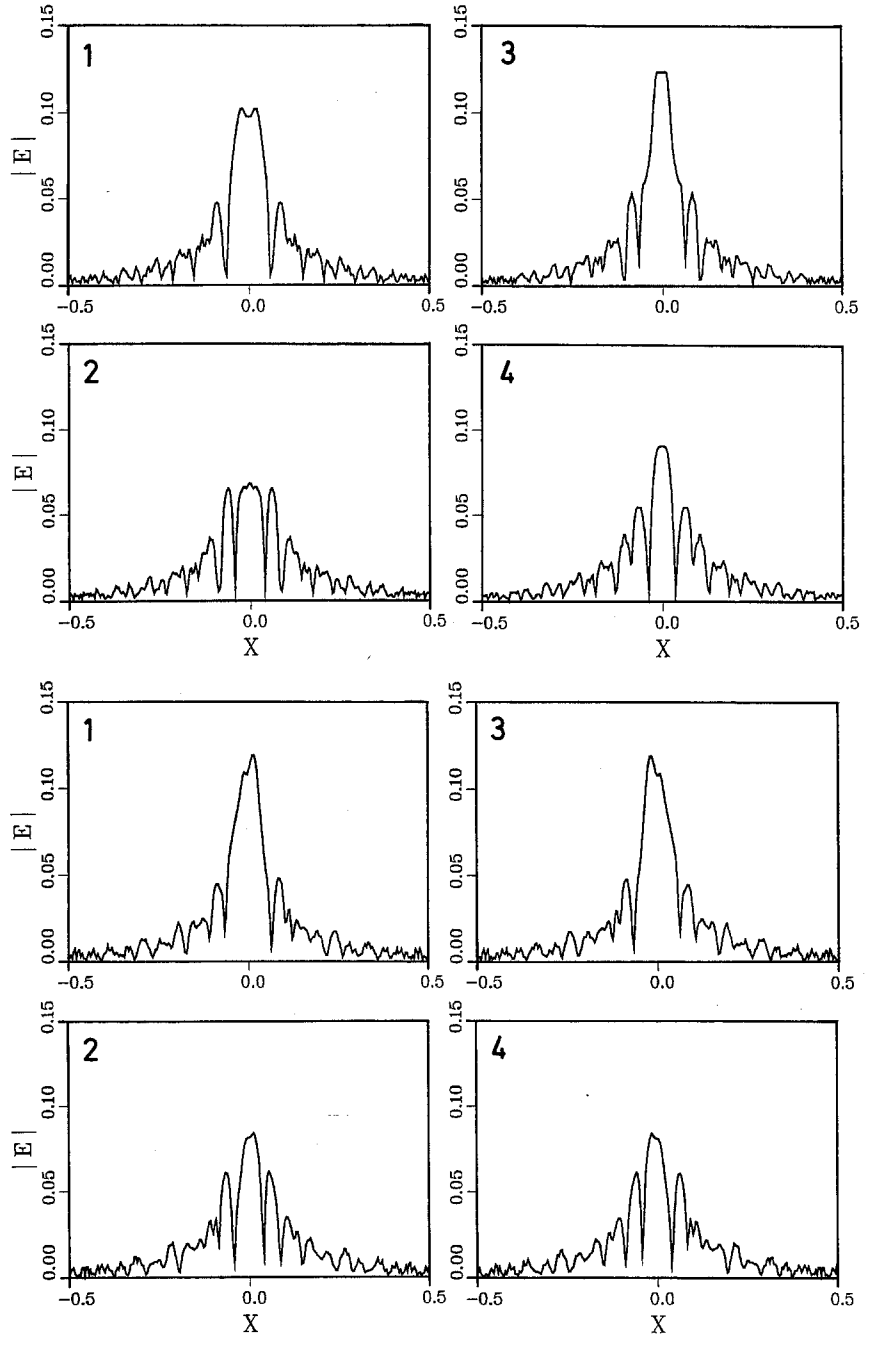

Fig. 5a, b. Steady P4 beam profiles obtained after 1000 round trips for **a** Crank-Nicholson method, **b** beam propagation method. Numbers 1–4 denote the order in which the profiles repeat

symmetry breaking of the allowed modes. Some modes of the system break the $x \rightarrow -x$ symmetry inherent in the model and some remain symmetric. Spontaneous breaking of spatial symmetries can lead to the coexistence of various attractors. Such phenomena are experimentally observed. It is with respect to this behavior that the methods differ.

One such instance is observed in the P4 solution which is formed for the aforementioned values of the parameters. The differences are not that much pronounced in the beam profiles, but in the fact that the CN mode remains symmetric, while the FFT is symmetry-broken. This is visible in Fig. 5. The *dancing* FFT mode could be more properly denoted as the P4–P2 solution, since the profiles are pair-wise mirror images of each other.

Figure 6 presents the time signal of the tip of the beam for both methods. It displays how the beams settle into steady-state profiles. While initially they go through similar dynamical phases (though with different time constants), the symmetry breaking transition is missing in the CN beam. The profiles of both beams at $N = 200$ round-trip times (not shown) are very similar and both are symmetric, however, then the FFT profiles undergo a slow transition to an asymmetric mode and remains as such.

The point to display is not that the FFT method is superior to CN. They are both more or less equally wrong for unstable or chaotic systems. The point is to become aware of the shortcomings of numerical methods when describing long-time behavior of unstable and/or chaotic systems. Applying

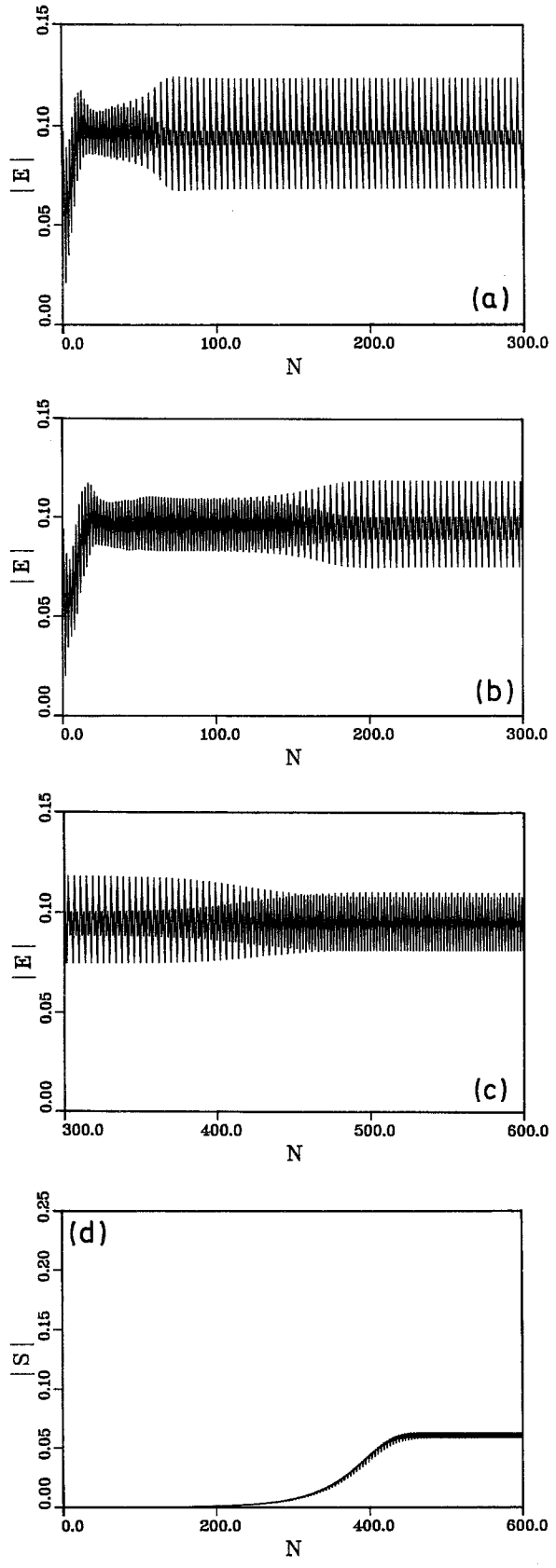

Fig. 6a–d. Time series of the tip of the beam for **a** CN method, and **b** FFT method, after $N = 300$ round trips. **c** The continuation of the time series for the FFT method. The system switches from a symmetric to an asymmetric mode. **d** Time series of the symmetry breaking parameter S, the integrated difference between the left and the right side of the profile (FFT method)

independent numerical methods can help understanding of the underlying model.

We should note in passing that the plane wave Ikeda model with round-trip time iterations has been compared by Le Berre et al. [13] to the Ikeda model with time-delay. Both models are derived from the same physical system. They found that the two show considerable differences in the unstable behavior and, particularly, that the map model leads to erroneous conclusions about the route to chaos and the dimension of attractors.

4 Conclusions

The overall conclusion is that different numerical approximations of the same physical system may lead to different results depending on the numerical scheme applied. Long-time behavior is difficult to predict accurately in unstable or chaotic systems. Sooner or later exponential separation of initially close points on a trajectory encompasses any finite accuracy tolerance, no matter how small it is.

Another conflicting requirement is that in order to follow motion near bifurcation points or on a strange attractor, long observation times are necessary, whereas for accuracy to be maintained, small integration steps must be chosen. Small tolerances that initially have to be set up translate into finite intervals in which the results can be trusted, and this contradicts the requirement $t \to \infty$ built-in in the definition of most chaotic phenomena. The behavior at $t \to \infty$ can not be properly investigated by numerical schemes which require $\Delta t \to 0$.

Simple as they are, these facts are often overlooked. No numerical algorithm can predict accurately the state of a chaotic system after a long period of time. Unpredictability is the essential feature of deterministic chaos. Even though the fundamental purpose of a numerical simulation of dynamical systems is to provide for their temporal evolution, the following of chaotic trajectories often is meaningless. Nonetheless, progress has been made recently along these lines by the introduction of shadowing techniques [14].

In spite of reservations mentioned above, the models introduced here, each on its own, represent interesting examples of nonlinear dynamical models. The disturbing fact that they show different long-time behavior when treated by different numerical methods is of little relevance. In other words, different numerical algorithms used to treat the same physical system may introduce dynamical models with vastly different behavior. On the level of models it is impossible to decide which one is better or more accurate in describing chaotic behavior. Qualitatively, they all give similar results, and in detail they are all wrong. Their relevance to the real, physical world can not be assessed properly without experimental evidence.

References

1. H.G. Schuster: *Deterministic Chaos* (Physikverlag, Weinheim 1988)
   H. Bai-Lin: *Elementary Symbolic Dynamics* (World Scientific, Singapore 1989)
2. For an overview of numerical methods applicable to chaotic systems, see for example: T.S. Parker, L.O. Chua: *Practical Numerical Algorithms for Chaotic Systems* (Springer, New York 1989)

3. M. Yamaguti, S. Ushiki: Physica D **3**, 618 (1981)
4. P. Günter, J.P. Huignard (eds.): *Photorefractive Materials and Their Applications* I and II, Topics Appl. Phys. Vol. **61** and Vol. **62** (Springer, Berlin, Heidelberg 1988, 1989)
5. K. Ikeda: Opt. Commun. **30**, 257 (1979)
6. M. Lax et al.: J. Opt. Soc. Am. A **2**, 731 (1985)
7. W. Krolikowski, M.R. Belić, M. Cronin-Golomb, A. Bledowski, J. Opt. Soc. Am. B **7**, 1204 (1990)
8. N.V. Kukhtarev, V. Markov, S. Odulov: Opt. Commun. **23**, 338 (1977)
9. M. Belić, D. Timotijevic, W. Krolikowski: J. Opt. Soc. Am. B **8**, 1723 (1991)
10. "Discussion on the existence and uniqueness or multiplicity of solutions of the aerodynamical equations", In: J. von Neumann Collected Works (Pergamon, Oxford 1961–1963) Vol. 6, p. 348
11. M. Sauer, F. Kaiser: Appl. Phys. B **55**, 138–143 (1992)
12. L. Lugiato, R. Lefever: Phys. Rev. Lett. **58**, 2209 (1987)
13. M. Le Berre, E. Ressayre, A. Tallet, H.M. Gibbs: Phys. Rev. Lett. **56**, 274 (1986)
14. C. Grebogi, S.M. Hammel, J.A. Yorke, T. Sauer: Phys. Rev. Lett. **65**, 1527 (1990)